Morphology, Thermal, and Mechanical Properties of Polyamide 66/Clay Nanocomposites with Epoxy-Modified Organoclay

Park Min Gyoo, Sriram Venkataramani,* Sung Chul Kim

Department of Chemical and Bimolecular Engineering, Centre for Advanced Functional Polymers, Korea Advanced Institute of Science and Technology, Yuseong-Gu, Daejeon 305–701, South Korea

Received 20 June 2005; accepted 26 September 2005
DOI 10.1002/app.23339
Published online in Wiley InterScience (www.interscience.wiley.com).

ABSTRACT: A new kind of organophilic clay, cotreated by methyl tallow bis-2-hydroxyethyl quaternary ammonium and epoxy resin into sodium montmorillonite (to form a strong interaction with polyamide 66 matrix), was prepared and used in preparing PA66/clay nanocomposites (PA66CN) via melt-compounding method. Three different types of organic clays, CL30B–E00, CL30B–E12, and CL30B–E23, were used to study the effect of epoxy resin in PA66CN. The morphological, mechanical, and thermal properties have been studied using X-ray diffraction, transmission electron microscopy (TEM), mechanical, and thermal analysis, respectively. TEM analysis of the nanocomposites shows that most of the silicate layers were exfoliated to individual layers and to some thin stacks containing a few layers. PA66CX–E00 and PA66CX–E12 had nearly exfoliated structures in agreement with the SAXS results, while PA66CX–E23 shows a coexistence of intercalated and exfoliated structures. The storage modulus of PA66 nanocomposites was higher than that of the neat PA66 in the whole range of tested temperature. On the other hand, the magnitude of the loss tangent peak in α- or β-transition region decreased gradually with the increase in the clay loading. Multiple melting behavior in PA66 was also observed. Thermal stability more or less decreased with an increasing inorganic content. Young's modulus and tensile strength were enhanced by introducing organoclay. Among the three types of nanocomposites prepared, PA66CX–E12 showed the highest improvement in properties, while PA66CX–E23 showed properties inferior to that of PA66CX–E00 without epoxy resin. In conclusion, an optimum amount of epoxy resin is required to form the strong interaction with the amide group of PA66. © 2006 Wiley Periodicals, Inc. J Appl Polym Sci 101: 1711–1722, 2006

Key words: organoclay; clay nanocomposites; polyamide 66; morphology; thermal stability; crystallization temperature

INTRODUCTION

Clay/polymer nanocomposites are the typical examples of nanotechnology, which offers tremendous improvement in a wide range of physical and engineering properties for polymers with low filler loading. This technology can now be applied commercially and has received great attention in recent years. Polyamide 6/clay nanocomposites (PA6CN) may be most successful polymer/clay nanocomposites (PCN) that have attracted a great deal of interest over the last few years as a result of the potentially superior properties compared to those of the conventional composites. Numerous studies have shown that even very low percentage of layered silicates can lead to a significant enhancement of many properties, such as stiffness and strength,[1,2] flame retardancy,[3,4] gas barrier properties,[5,6] ionic conductivity,[7,8] thermal stability,[9] and tunable biodegradability.[2] All these properties make these materials interesting prospects for a wide variety of applications, such as in automotive, electronics, food packaging, biotechnology, and many others.

Work from the Toyota research laboratories sparked a large interest in PA6CN. Their research studies describe PA6CN made by an *in situ* polymerization process, which exhibited superior strength, modulus, heat distortion temperature, and water and gas barrier properties with respect to virgin PA6.[10–14] Their results indicate that this process leads to a large number of polyamide molecules, in their PA6CN, that are ion-bonded to the silicate layers via the protonated amine chain ends, —NH_3^+, and that the enhancement in mechanical properties were correlated to the large surface area and to the ionic bonds between the organic polymer and the inorganic silicate.[15,16]

Interestingly, PA6CN prepared by melt compounding using a twin screw extruder show comparable properties to those prepared by the *in situ* technique.[17] In melt compounding, one would not expect the amine to be protonated, because it is only a physical

Correspondence to: S. C. Kim (kimsc@kaist.ac.kr).
**Present address:* Aortech Biomaterials Pty Ltd, Melbourne, Australia.

Contract grant sponsor: Korean Ministry of Science and Technology.

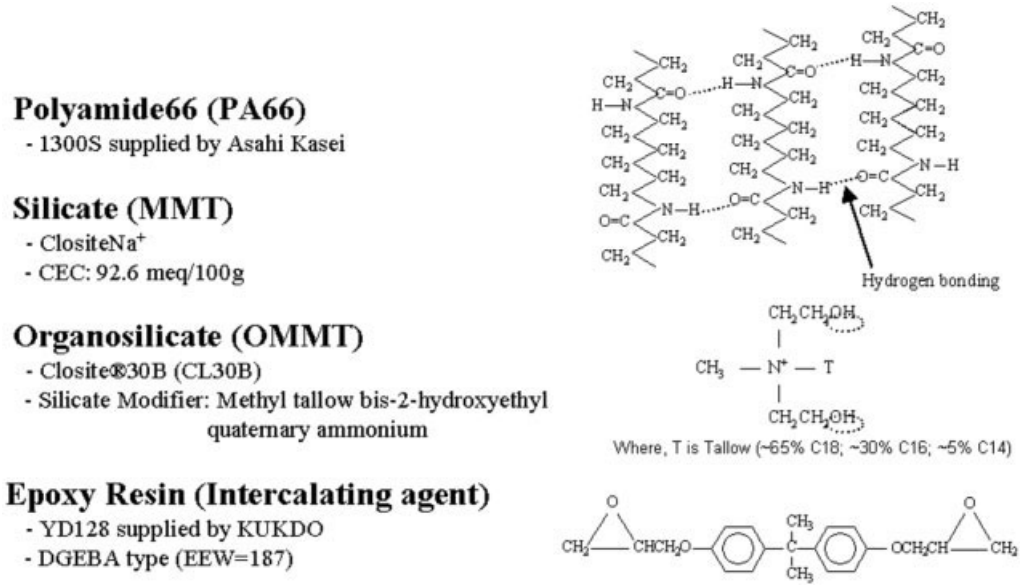

Figure 1 Chemical structure of materials used in this study.

blending process. Despite that, a comparable enhancement in properties is obtained. This preparation process is of great interest because of its enormous advantages for the commercial production of these materials, as has been pointed out in the literature.[17,18] These prior studies show that the melt viscosity and the residence time in the extruder are very important to obtain a well-exfoliated structure. The degree of exfoliation of the organoclay in the polymer matrix has a direct effect on the modulus and the strength of the nanocomposite.[17] Matrices with higher molecular weight produce a higher degree of exfoliation, which improves composite properties such as stiffness and strength, with a marginal loss of ductility.[18] This phenomenon is attributed to the higher melt viscosity which translates to a higher shear stress imposed on clay particles inside the extruder.

Polyamide 66 (PA66) is a kind of important engineering plastic. Despite PA6 and PA12/clay nanocomposites that have been investigated, there are only very few literature concerning PA66 nanocomposites (PA66CN), including the works by Goettler et al.[19,20] that analyze the effect of compounding method, molecular weight, amine/carboxyl end group ratio, and cation-exchange capacity of the organoclay on the mechanical properties of nanocomposites made with PA6, PA66, blends, and copolymers of PA6 and PA66. Some other studies on the hydrogen bonding, crystallization behavior, thermal stability and flammability, mechanical properties, morphology, and molecular modeling of PA66CN were reported.[21–31]

In this study, we prepare a new kind of organophilic montmorillonite, cotreated by methyl tallow bis-2-hydroxyethyl quaternary ammonium and epoxy resin, which can form a strong interaction with PA66 matrix. The organoclays were incorporated to PA66CN via melt compounding method. It is expected that the alkyl ammonium makes the silicate layers organophilic, and then epoxy groups between the layers attract PA66 molecules and cause strongly increased layer separation. To study the effect of epoxy resin in PA66CN, three different types of organoclays were prepared and compared, and named as CL30B–E00, CL30B–E12, and CL30B–E23, respectively. The effects of the organoclays on the properties of the PA66 nanocomposites, such as the morphology, dynamic mechanical properties, crystal structure and crystallization behavior, glass transition temperature, thermal stability, and tensile properties were also investigated and analyzed.

EXPERIMENTAL

Materials

Polyamide 66 with grade of 1300S was manufactured by Asahi Kasei. Cloisite®30B (Southern Clay Products, Inc.) was used as organoclay without further purification; it was formed by a cation-exchange reaction between sodium montmorillonite and methyl tallow bis-2-hydroxyl quaternary ammonium, and particle size was less than 20 μm. Epoxy resin, YD128, a diglycidyl ether of bisphenol A with an epoxide equivalent weight of 187 was kindly supplied by Kukdo Chemical Co., Korea, which acts as a reactive intercalating agent with PA66. The abbreviations and chemical structures are described in Figure 1. In addition, all data are indicated in terms of weight percent inorganic content (wt % MMT) in the PA66 nanocomposites, rather than the amount of organoclay, since the silicate is the reinforcing component.

TABLE I
The Weight Percent of Components in Cloisite30B–Epoxy Mixture

	Sample code	Inorganic content (wt %)	Organifier[a] content (wt %)	Epoxy content (wt %)
Type I	CL30B-E00	68.9	31.1	—
Type II	CL30B-E12	62.0	26.4	11.6
Type III	CL30B-E23	54.0	23.3	22.7

[a] Methyl tallow bis-2-hydroxyethyl quaternary ammonium.

Preparation of Cloisite30B–epoxy mixture

Cloisite30B–epoxy mixtures were prepared using a corotating brabender mixer at 80°C with rotor speed of 100 rpm for 1 h. There are three kinds of compounding types: Type I, Type II, and Type III. In case of Type I, only 20 g of Cloisite30B was mixed in brabender mixer without using an epoxy resin. In Type II, 17 g Cloisite30B was mixed with 3 g of epoxy resin, and in Type III, 15 g Cloisite30B was mixed with 5 g of epoxy resin. Based on the residual weight in the thermogravimetric analysis (TGA) thermogram, the weight percent of each component was calculated. First, the weight percent of inorganic and organifier content in Cloisite30B–epoxy mixture was calculated, and then the weight percent of the pure epoxy resin incorporated into the organoclay was determined. The results are tabulated in Table I.

Preparation of polyamide 66/clay nanocomposites

Prior to each processing step, all PA66 samples were dried in vacuum oven for 48 h at 80°C to avoid moisture-induced degradation reactions, and then blended with Cloisite30B–epoxy mixture. Composites were prepared by melt compounding using a brabender mixer at 265°C under N_2 atmosphere. The rotor speed of brabender mixer was maintained at 100 rpm for 10 min. After drying at 80°C for 48 h, the obtained nanocomposites were compression molded to get test specimens for measurement of dynamic mechanical and tensile properties. For comparison, neat PA66 was also prepared in the brabender mixer at the same processing conditions.

Characterization

Morphological analysis

To determine the dispersibility of organoclay in PA66 matrix, the scanning electron microscopy (SEM) studies were carried out. SEM specimens were prepared by O_2 plasma etching technique. The nanocomposite was plasma-etched for 10 min under O_2 atmosphere. The surface of the plasma-etched nanocomposite was observed by using a Jeol JSM-5610 SEM after gold coating to determine the dispersibility of organoclay. Wide-angle X-ray diffraction (WAXD) was conducted at ambient temperature on Rigaku D/Max-RC diffractometer with Cu Kα radiation (λ = 0.15418 nm) to measure the d-spacing of organoclays in PA66 matrix and change of crystal structure with different clay content. The d-spacing of organoclays was calculated by using Bragg's equation, according to the angle of (001) diffraction peak; $2d \sin \theta = \lambda$, where λ corresponds to the wave length of the X-ray radiation used in the diffraction experiment, d corresponds to the spacing between diffraction lattice planes, and θ is the measured half-diffraction angle or glancing angle. Each sample was scanned from 2θ = 1.2° to 30° at a scan rate of 2°/min. For comparison, WAXD patterns of pristine MMT and organoclay were carried out in the range from 2θ = 1.2° to 10°. The pattern of small-angle X-ray scattering (SAXS) was measured by using a Rigaku SWXD in measurement range from 2θ = 0.3° to 6.0°. The specimens for transmission electron microscopy (TEM) observation were prepared by using a RMC MT-XL microtome with cryogenic CR-XL system. The specimens were cut with a diamond knife at −80°C into the thickness of about 100 nm. TEM micrographs were obtained by using a Phillips CM20 transmission electron microscopy.

Dynamic mechanical properties

Temperature dependence of elastic storage modulus and loss tangent delta was measured by using a Rheometric Scientific DMTA IV. DMTA experiments were made at a fixed frequency of 1 Hz with a heating rate of 2°C/min over a temperature range of −120 to 150°C in three-point bending mode.

Thermal properties

The thermal properties of PA66 and the various composites were determined by differential scanning calorimetry (DSC) and TGA.

The DSC measurements were performed under nitrogen atmosphere by using a TA instruments DSC Q100 to measure the melting temperature (T_m), heat of fusion (ΔH_m), crystallization temperature (T_c), heat of crystallization (ΔH_c), and glass transition temperature (T_g) of

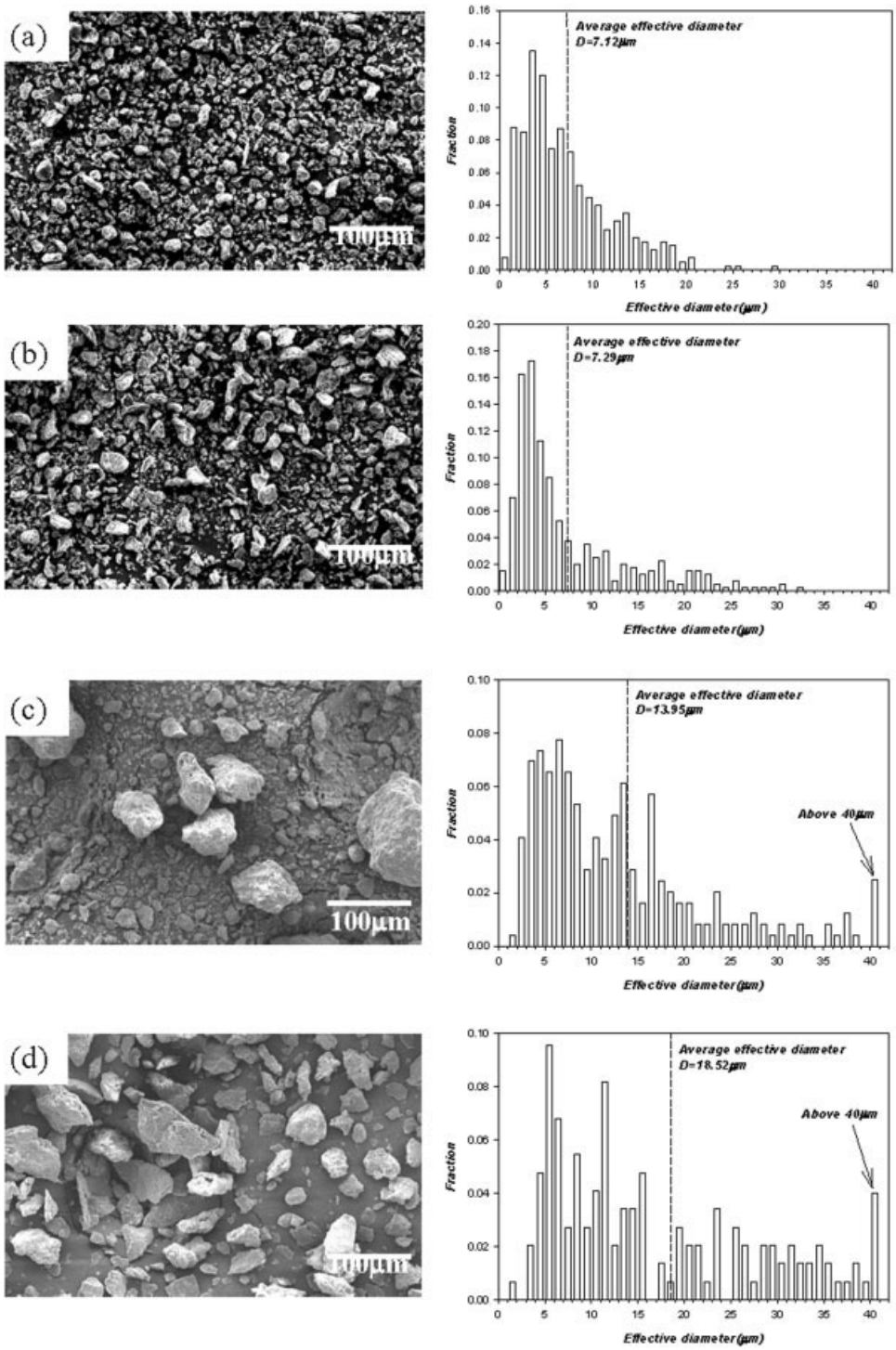

Figure 2 SEM micrographs and size distribution of clay particles (a) CloisiteNa^+ organoclay, (b) CL30B–E00, (c) CL30B–E12, and (d) CL30B–E23.

PA66 and PA66CN. The measurement was first carried out by heating the sample from −80 to 280°C and holding for 15 min to eliminate the residual crystals, cooling to −80°C at a rate of 10°C/min to record the cooling process, and then heating the sample from −80 to 280°C at 10°C/min to record the melting process.

Thermogravimetric analysis was performed under nitrogen atmosphere by using a TA Instruments TGA Q500 to measure the thermal stability of PA66 and PA66CN. The measurement was conducted with a heating rate of 20°C/min in the temperature range of 50–900°C.

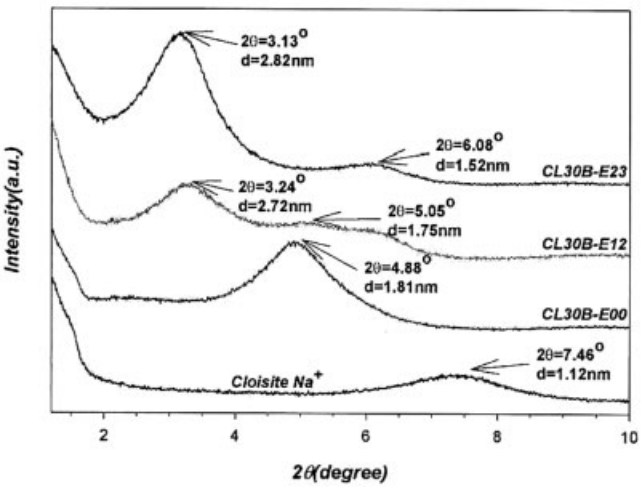

Figure 3 XRD patterns of CloisiteNa$^+$, CL30B–E00, CL30B–E12, and CL30B–E23.

Tensile properties

Tensile test was carried out with an Instron 5583 machine, according to ASTM D638M. The crosshead speed was 1 mm/min.

Notation

Code for organoclays

Cloisite30B and epoxy resin were used as commercialized organoclay and intercalating agent, respectively. "CL30B" and "E" indicate the code for Cloisite30B and epoxy resin, respectively. The last number indicates the weight percent of Epoxy resin in Cloisite30B–epoxy mixture. For example, CL30B–E12 means the Cloisite30B–epoxy mixture containing 12 wt % epoxy resin as intercalating agent (so, Cloisite30B : epoxy = 88 : 12).

Code for nanocomposites

The first word "PA66" indicates the polyamide 66. The following letter "C" indicates "clay (inorganic content)," and the following number represents the weight percent of inorganic content in PA66CN. The last codes for epoxy resins were the same as the second codes used for organoclay. For example, PA66C2–E12 means PA66 nanocomposites with 2 wt % inorganic content prepared with Cloisite30B–epoxy mixture containing 12 wt % epoxy resin.

RESULTS AND DISCUSSION

Morphology of organoclays

Figure 2 shows SEM micrographs of pristine montmorillonites and organoclays. Cloisite®Na$^+$ had small clay particles ranging from 1 to 30 μm as shown in Figure 2(a) and 7.12 μm of average effective diameter. CL30B–E00 were also having small clay particles with an average effective diameter of 7.29 μm. On the other hand, some portions of large agglomerated particles above 40 μm were visible in the micrograph of CL30B–E12 and CL30B–E23 as described in Figures 2(c) and 2(d). The average effective diameters were 13.95 and 18.52 μm, respectively. With an increase of epoxy content, particle size of epoxy-treated organoclay was gradually increased.

Figure 3 shows the X-ray diffraction (XRD) patterns for CloisiteNa$^+$, Cloisite®30B, organoclay treated with epoxy resins. The peak of basal spacing of CloisiteNa$^+$ appeared at $2\theta = 7.46°$ corresponding to $d = 1.12$ nm. After the treatment of organifier, the peak of basal spacing was shifted toward lower angle. In case of CL30B–E00 without epoxy content, the d-spacing was increased by 0.69 nm compared with that of pristine MMT. The cation exchange of Na^+ to quaternary ammonium expanded the interlayer space. With the introduction of epoxy resin, the d-spacing was increased more. The basal spacing of CL30B–E12 and CL30B–E23 was 2.72 and 2.82 nm, respectively, showing the increase of 0.91 and 1.01 nm as compared with that of CL30B–E00. These results could be explained by an intercalation of epoxy resin into silicate layers. The alkyl ammonium ion exchange enabled the conversion of the hydrophilic interior clay surface to hydrophobic and increased the layer distance as well. In this organophilic environment, epoxy resin could diffuse into the clay galleries to increase the layer distance further. In addition to the increase in layer distance, it was expected that the introduction of epoxy resin would also bring the active functional group into PA66 system.

Dispersibility of organoclay in PA66 matrix

Figure 4 shows the representative SEM micrograph and size distribution of clay particles of O_2 plasma-etched PA66CX–E23. The number of agglomerated clay particles increased with an increase in clay loading. It also shows an increasing number of residual clusters above 10 μm, and PA66CX–E23 had 2.06–2.73 μm of average effective diameter. This is due to larger clay size than other systems (CL30B–E00 or CL30B–E12) studied.

Figures 5(a) and 5(b) show the representative WAXD patterns of PA66CX–E00 and PA66CX–E23, respectively. Two strong diffraction peaks at $2\theta = \sim 20°$ and $\sim 24°$ were observed for all the nanocomposites. Peaks at $2\theta = \sim 20°$ and $\sim 24°$ were assigned to (100) and (010, 110) planes of the α-phase crystals of PA66, respectively.[32] From the WAXD patterns, it can be seen that with increasing the clay content, the positions of the diffraction peaks remained almost un-

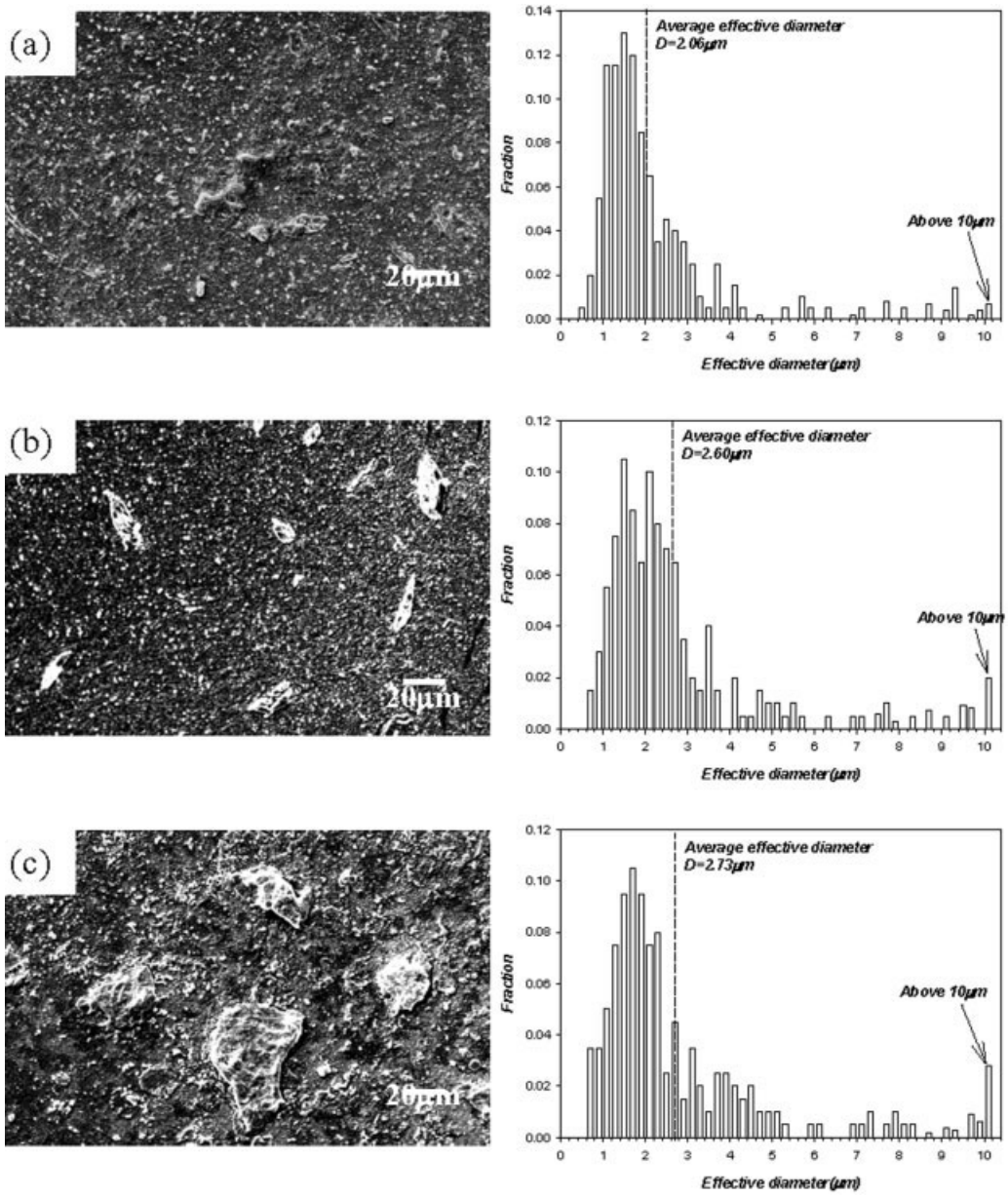

Figure 4 SEM micrographs and size distribution of clay particles of PA66CX–E23. (a) 2 wt %, (b) 4 wt %, and (c) 5 wt %.

changed, while the relative intensity of (010, 110)/(100) gradually increased. This probably indicates a preferential packing of the crystals (010, 110) plane, which can be induced by incorporation of clay platelets into PA66 matrix, since all the samples had the same thermal history.[33] Next, there were no peaks for basal spacing ranging from $2\theta = 1.2°–10°$ after preparing PA66 nanocomposites. For instance, in case of PA66CX–E00, no peaks were observed in the range of $2\theta = 1.2°–10°$, while the peak of CL30B–E00 appeared at $2\theta = 4.88°$, corresponding to a basal plane spacing $d = 1.81$ nm. Similar results were also observed for PA66CX–E12 and PA66CX–E23. The absence of the characteristic d_{001} diffraction peak of clay is the strong evidence for the formation of exfoliated or disordered nanocomposites. It can be explained as the introduction of polar group such as —OH along the chain of quaternary ammonium in silicate modifier can increase the potential binding energy with polar polymer such as PA66, it makes the intercalation of PA66 molecules into the gallery easy. In addition, the epoxide groups of epoxy resin can react with amide group of the PA66; so, it is expected to further enhance the dispersion. However, in Figure 5(b), the WAXD pattern of PA66C5–E23, small but broad peak, was observed around $2\theta = 2.5°$. It implies that PA66CX–E23 formed an intercalated structure with some disorder.

In the WAXD patterns of nanocomposites, there were no peaks for basal spacing ranging from $2\theta = 1.2°$ to 10°. In SAXS patterns shown, the d-spacing of

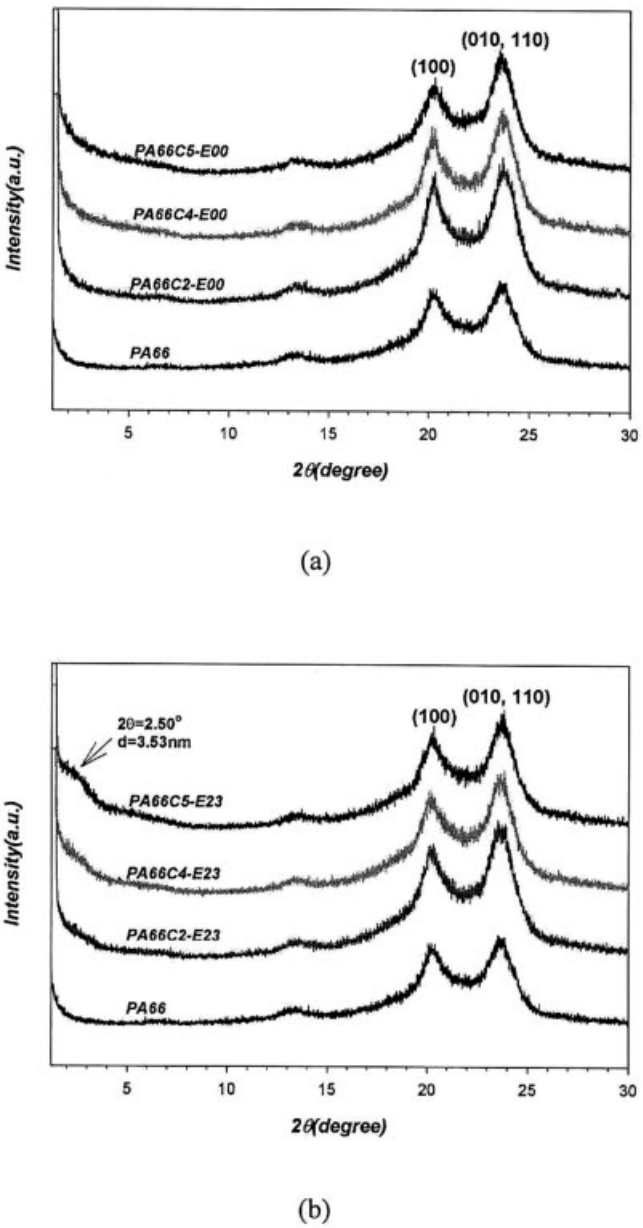

Figure 5 WAXD patterns of nanocomposites (a) PA66CX–E00 and (b) PA66CX–E23.

CL30B–E00 was 1.81 nm corresponding to $2\theta = 4.88°$, while the diffraction peaks at $2\theta = 0.93°$, 0.92°, and 0.90°, corresponding to *d*-spacing of 9.44, 9.54, and 9.75 nm, appeared for PA66C2–E00, PA66C4–E00, and PA66C5–E00, respectively. The *d*-spacings of PA66CX–E00 were about 7.63–7.94 nm higher than that of CL30B–E00. In case of nanocomposites prepared using CL30B–E12 as organoclay, the peaks for basal spacing were shifted toward a little lower angle. The *d*-spacings corresponding to $2\theta = 0.94°$, 0.89°, and 0.87° were 9.31, 9.86, and 10.15 nm, respectively, and the intensity of peaks gradually decreased with an increase in clay loading. However, it is not clear whether these peaks appearing around $2\theta = 1.0°$ reflect the basal spacing of the organoclay, because the peak of long-range order attributed to the lamellae structure of neat PA66 is also shown in $2\theta = 1.03°$. The SAXS patterns of PA66CX–E23 (Fig. 6), on the other hand, revealed low broad peaks in the range of $2\theta = 2.24°$–2.59°, corresponding to basal spacing of 3.40–3.93 nm. These peaks could be caused by the intercalation of PA66 molecules into silicate layers, which results from a strong interaction between hydroxyl group of silicate modifier and epoxide group of epoxy resin. Therefore, the intercalated layer shows somewhat expanded gallery spacing when compared to the organoclay itself. It seems that the nanocomposite consisted of the mixture of the intercalated platelet assembly as well as partially exfoliated clay dispersion (with 9–10 nm gallery spacing).

Representative TEM micrographs of PA66C2–E00, PA66C2–E12, and PA66C2–E23 are shown in Figure 7. The dark lines represent the intersection of MMT layers and the white background represents PA66 matrix. It was seen that MMT layers were partially exfoliated to individual layers or to some thin stacks containing a few layers. PA66C2–E00 and PA66C2–E12 had nearly exfoliated structures in agreement with the SAXS results, while PA66C2–E23 revealed a mixture of intercalated and exfoliated structures. Similar results are observed in higher percentage of clay nanocomposites. For a more complete analysis on the exfoliation of the organoclay in these polymer matrices, quantitative analyses of dispersed or stacked platelets in TEM photomicrographs (low magnification) were conducted. Image analysis data, given in Table II, provides a quantitative comparison between the different composites. The particle population, which is the average number of particles per μm^2, is a measure of the extent of exfoliation with average thickness of platelets and standard deviation of thickness. As seen in Table II, PA66CX–E00 and PA66CX–E12 showed

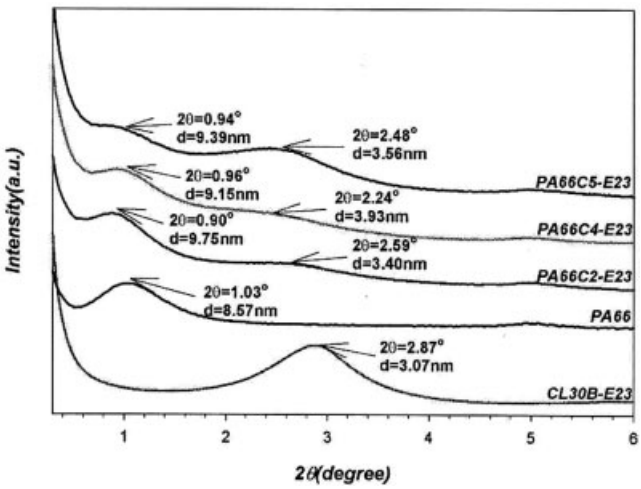

Figure 6 SAXS patterns of PA66CX–E23 nanocomposites.

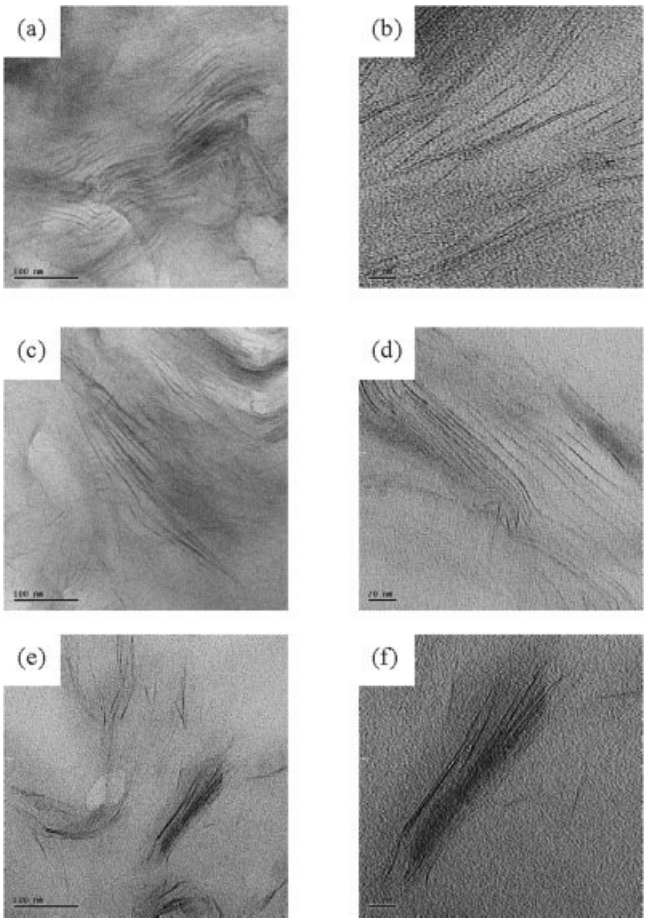

Figure 7 TEM micrographs of PA66C2–E00 (a) low magnification, (b) high magnification; PA66C2–E12 (c) low magnification, (d) high magnification; and PA66C2–E23 (e) low magnification, (f) high magnification.

higher values than those PA66CX–E23 showed in particle population. Also, PA66CX–E12 showed the lowest value in average thickness and standard deviation

TABLE II
TEM Analysis Results of PA66 Clay Nanocomposites

	Inorganic content (%)		
	2	4	5
Particle population[a]			
PA66CX-E00	49	57	65
PA66CX-E12	58	64	69
PA66CX-E23	23	42	51
Average thickness			
PA66CX-E00	4.77	5.24	6.06
PA66CX-E12	3.43	4.53	4.70
PA66CX-E23	5.62	6.75	7.35
Standard deviation			
PA66CX-E00	3.03	3.49	5.06
PA66CX-E12	2.24	2.46	3.58
PA66CX-E23	6.66	9.54	10.99

[a] The particle population is the average number of momtmorillonite particles per μm^2.

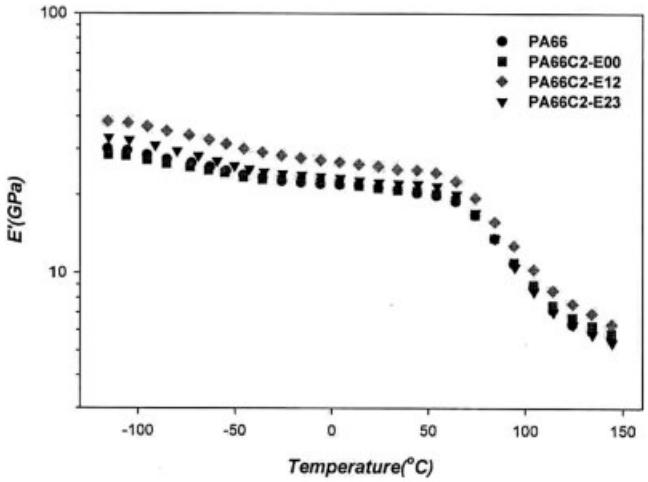

Figure 8 Temperature dependence of storage modulus of PA66C2–EXX.

of thickness. For PA66CX–E12, the organoclay was well dispersed to individual platelets in PA66 matrix. On the other hand, the PA66CX–E23 showed low particle population, accompanying high average thickness and standard deviation of thickness. The dispersibility of organoclay in PA66 matrix is in agreement with TEM image results. This difference in morphology will affect various properties such as dynamic mechanical properties, tensile properties, and thermal properties.

Dynamic mechanical properties

The storage modulus (E') decreased monotonously with increasing temperature in the range of -120 to 50°C, and there was a sharp decrease near the T_g (α-transition), which occurs due to main chain motion, and β-transition around 50°C, which occurs due to side-chain motion. Clearly, inorganic MMT increased the storage modulus of PA66. In case of PA66CX–E12, especially, only a low percent of inorganic clay (2 wt %) gave remarkable increases in stiffness. As seen in Figure 8, the storage modulus of PA66C2–E12 was higher than those of other nanocomposites with the same inorganic content of 2 wt %. The improvement in the storage modulus with small clay loading may result from the strong interaction between the organoclay and the PA66. It also reflects that silicate layers were well dispersed in PA66 matrix.

Thermal properties

Crystal structure and crystallization behavior

The glass transition temperature (T_g), melting temperature (T_m), heat of fusion (ΔH_m), crystallization temperature (T_c), heat of crystallization (ΔH_c), and crys-

TABLE III
Thermal Properties of PA66 Clay Nanocomposites

	Inorganic content (%)			
	0	2	4	5
Glass transition temperature				
PA66CX-E00	60.7	59.1	59.0	59.8
PA66CX-E12	—	59.4	58.9	59.1
PA66CX-E23	—	59.4	58.6	59.3
Melting temperature				
PA66CX-E00	262.3	262.0	261.4	261.7
PA66CX-E12	—	261.7	260.6	261.1
PA66CX-E23	—	260.8	260.6	260.8
Crystallization temperature				
PA66CX-E00	59.4	68.1	65.3	62.9
PA66CX-E12	—	67.0	65.9	62.2
PA66CX-E23	—	65.4	62.6	59.0
Heat of crystallization				
PA66CX-E00	218.7	235.8	234.2	232.5
PA66CX-E12	—	234.8	233.4	231.5
PA66CX-E23	—	233.6	231.8	230.9
Crystallinity				
PA66CX-E00	30.3	34.7	33.3	32.1
PA66CX-E12	—	34.2	33.6	31.7
PA66CX-E23	—	33.3	31.9	30.1

tallinity of PA66 and PA66CN were determined and are summarized in Table III. The percent crystallinity of the PA66 samples was calculated as the ratio of the heat of fusion of the sample, with units of Joule per gram, to the heat of fusion of the pure crystalline form of PA66. The value for pure PA66 was taken as 195.9 J/g.[34]

The T_g values detected by DSC were lower than those detected by DMTA, due to the different heating rate and different frequency. As with DMTA results, the T_g from DSC also shows little change with increasing the clay contents. The melting point also shows similar value, irrespective of clay content. The formation of a small shoulder before the main endothermic peak (α-crystalline form) was associated with γ-crystalline form of PA66, as suggested by various researchers.[35–37]

The effect of the inorganic content on the crystallization behavior of PA66 was studied by DSC cooling scans. The presence of clay in the nanocomposites increased the crystallization temperature and narrowed the width of the crystalline peak. The clay increased the crystallization rate and had a strong heterophase nucleation effect on PA66. In other words, clay particles, at low concentration, served as nucleating agents that increase the rate of crystallization of the PA66 matrix. So, crystallization temperature of PA66 nanocomposites was increased by 15°C relative to that of neat PA66. However, at high concentrations of clay, the rate of crystallization was retarded, which reduced the crystallinity. The retardation of crystallization rate at high organoclay contents was more pronounced as the level of exfoliation and organoclay concentration increased. This may be the reason for the decrease in percent crystallinity as the clay loading increases, as shown in Table III. For example, crystallinity of neat PA66 was 30.3%, while that of PA66C2–E12, PA66C4–E12, and PA66C5–E12 were 34.2%, 33.6%, and 31.7%, respectively. This generally suggests that there is a high degree of exfoliation in the PA66 nanocomposites, which corroborates the mechanical properties.

Thermal stability

The representative TGA thermogram of PA66CX–E00 is shown in Figure 9, and TGA results are summarized in Table IV. Temperature at 5 wt % decomposition and maximum decomposition rate are indicated as T_{95} and

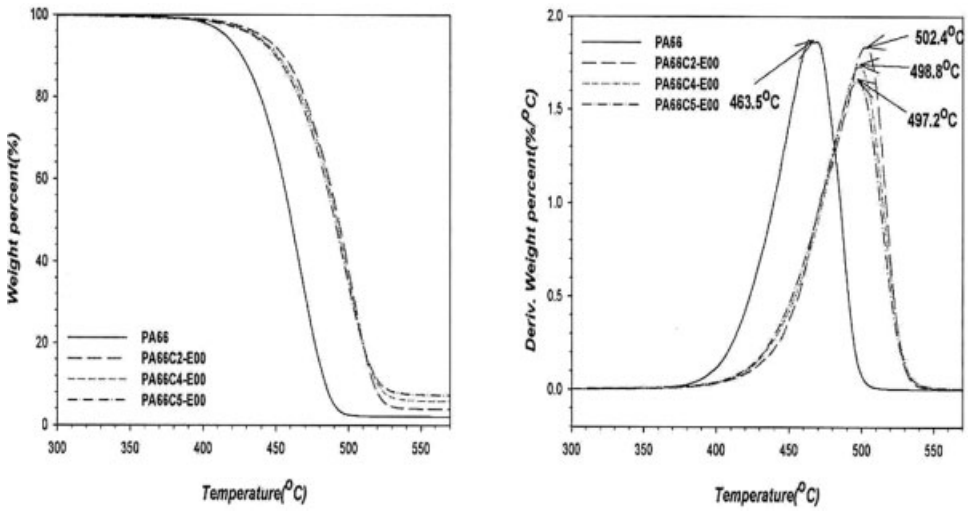

Figure 9 TGA thermogram of PA66CX–E00.

TABLE IV
TGA Results of PA66 Clay Nanocomposites

	Inorganic content (%)			
	0	2	4	5
T_{95}[a]				
PA66CX-E00	414.8	439.5	435.8	433.5
PA66CX-E12	—	438.1	434.0	432.5
PA66CX-E23	—	434.6	430.1	424.2
T_{max}[b]				
PA66CX-E00	463.5	502.4	498.8	497.2
PA66CX-E12	—	502.1	500.5	498.4
PA66CX-E23	—	498.1	495.0	490.4

[a] T_{95}, temperature at 5 wt % decomposition.
[b] T_{max}, temperature at maximum decomposition rate.

T_{max}, respectively. Generally, clay particles can enhance the thermal stability of polymer by acting as thermal insulator[38] and mass transport barrier[39] to the volatile products generated during decomposition. For all the nanocomposites, T_{95} and T_{max} were higher than those of neat PA66, but both T_{95} and T_{max} were slightly decreased with an increasing inorganic content. Remarkably, the weight percent of silicate modifier–epoxy in PA66 matrix also increased with the increase of inorganic content. The weight percent of organifier–epoxy in PA66 nanocomposites is listed in Table V. The onset temperature of decomposition of the surfactants was about 200°C, which may act as a shortcoming of the alkyl ammonium and epoxy-pretreated MMT when it was used to prepare polymer nanocomposites at higher melting compounding temperature. Vanderhart et al.[40] investigated the chemical stability of a dimethyl-di (hydrogenated tallow) ammonium MMT during melt blending with PA6 at 240°C. When such an MMT surface was exposed to PA6, most of the ammonium surfactant on that surface was decomposed, releasing a free amine with one methyl and two tallow substituents, which was caused by the combination of temperature and shear stress during melt blending. In this study, pristine MMT with polar hydroxyl end groups has good affinity for polar PA66 chains by polar and ionic interaction. Tanaka and Goettler,[31] however, reported that pristine

TABLE V
Organifier–Epoxy Weight Percent in PA66 Nanocomposites

	Inorganic content (%)		
	2	4	5
PA66CX-E00	0.90	1.80	2.25
PA66CX-E12	1.22 (0.37)[a]	2.44 (0.74)	3.05 (0.93)
PA66CX-E23	1.70 (0.84)	3.40 (1.68)	4.25 (2.10)

[a] Values in parentheses indicate the pure epoxy weight percent contained in PA66 nanocomposites.

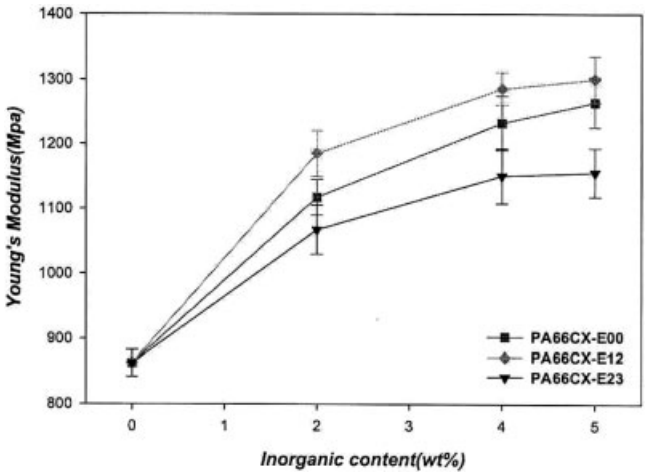

Figure 10 Young's modulus of PA66 clay nanocomposites.

MMT yields the highest binding strength to PA66, and the binding energy between PA66 and the MMT layer decreases almost linearly with an increasing content of alkyl ammonium surfactant. Because of these reasons, it is believed that T_{95} and T_{max} values of the PA66 nanocomposites exhibit a slight decrease with the increase of organoclay cotreated with silicate modifier and epoxy resin.

Static mechanical analysis

Representative young's modulus, tensile strength, and elongation at break for PA66CX–E00, PA66CX–E12, and PA66CX–E23 are shown in Figures 10–12, and the results are summarized in Table VI. For all nanocomposites, young's modulus increased with increasing the clay content. The addition of organoclay to the polymer matrix produced a substantial increase of the modulus in all types of PA66 nanocomposites, even at

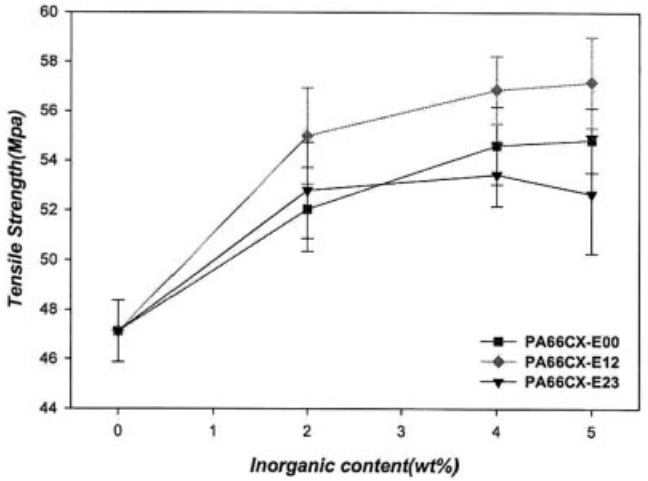

Figure 11 Tensile strength of PA66 clay nanocomposites.

low loadings (2 wt% MMT). The enhancement of Young's modulus is directly attributed to the reinforcement by the dispersed silicate layers[2] and to the strong interactions between matrix and silicate layers via the formation of hydrogen bonding.[41] The extent of the improvement of the modulus also depends upon the average length of the dispersed clay particles, and hence, aspect ratio,[10] which correlates well with the dispersity of organoclay. Young's modulus of PA66CX–E12 was higher than those of other nanocomposites: PA66CX–E00 and PA66CX–E23. The largest increase in Young's modulus (1.5 fold) was shown by PA66C5–E12. This is due to the strong interaction, such as curing reaction, between amide groups of PA66 molecules and epoxide groups tethered in the layered silicates. This is in good agreement with TEM results (Table II), which shows maximum particle population in PA66CX–E12. This interaction could be expected to increase the dispersibility of organoclay in PA66 matrix. In spite of containing more epoxy contents, PA66CX–E23 showed inferior properties than the nanocomposite without epoxy resin, PA66CX–E00. This is because epoxy resin does not give any active sites in the PA66 matrix by a strong interaction between diepoxide group of epoxy resin and dihydroxyl group in the silicate modifier, as shown in SAX pattern. In other words, epoxy resin may not act as crosslinkable agent on PA66. Tensile strength also showed a similar behavior as Young's modulus. In addition, Young's modulus and tensile strength of PA66 nanocomposites deviated from linearity at high levels of MMT. Nonlinear trends such as this may stem from the fact that, for PA66, the ability to exfoliate the clay decreases as the loading increases. In other words, it is the result of the inevitable aggregation of the layers in high clay content. The effect of inorganic content on the elongation at break is shown in Figure 12. Elongation at break decreased rapidly with loading of 2 wt % inorganic content, but changed little for loading higher than 2 wt % inorganic content. It is attributed to the stiffness and large aspect ratio of silicate layers.

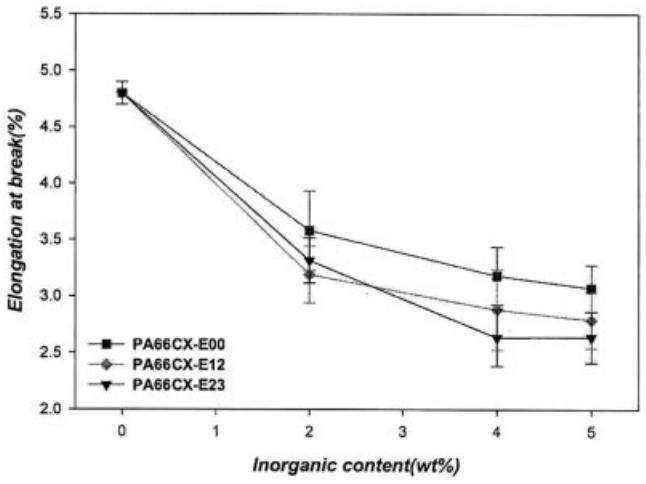

Figure 12 Elongation at break of PA66 clay nanocomposites.

TABLE VI
Static Mechanical Properties of PA66 and PA66 Clay Nanocomposites

Inorganic content	Young's modulus (MPa)	Tensile strength (MPa)	Elongation at break (%)
PA66			
0 wt %	862.60 ± 20.50	47.13 ± 1.25	4.8 ± 0.10
PA66CX-E00			
2 wt %	1117.14 ± 27.46	52.04 ± 1.69	3.58 ± 0.35
4 wt %	1232.66 ± 42.25	54.62 ± 1.58	3.18 ± 0.26
5 wt %	1264.25 ± 38.64	54.84 ± 1.31	3.07 ± 0.21
PA66CX-E12			
2 wt %	1184.74 ± 35.46	55.00 ± 1.95	3.19 ± 0.25
4 wt %	1285.79 ± 25.04	56.87 ± 1.37	2.88 ± 0.35
5 wt %	1300.08 ± 35.34	57.17 ± 1.84	2.79 ± 0.25
PA66CX-E23			
2 wt %	1067.23 ± 37.84	52.80 ± 1.94	3.31 ± 0.20
4 wt %	1150.23 ± 42.70	53.44 ± 1.28	2.63 ± 0.25
5 wt %	1155.45 ± 37.88	52.66 ± 2.39	2.64 ± 0.23

CONCLUSIONS

A new kind of organophilic clay was obtained through cointercalation of methyl tallow bis-2-hydroxyethyl quaternary ammonium and epoxy resin into sodium montmorillonite. PA66CN were prepared with this kind of organophilic clay by melt intercalation. From TEM images of the prepared nanocomposite system states, it is seen that most of the silicate layers were exfoliated to individual layers or some thin stacks containing a few layers. PA66CX–E00 and PA66CX–E12 had nearly exfoliated structures in agreement with the SAXS results, while PA66CX–E23 revealed a mixture of intercalated and exfoliated structures. The excess of epoxy resin could cause a strong reaction with hydroxyl end groups of silicate modifier on the silicate surface, and so limit the diffusion of PA66 molecules into silicate layers. Dynamic mechanical study reveals that the storage modulus (E') decreased monotonously with increase in the temperature from -120 to 80°C and had a sharp decrease near the T_g. The storage modulus of PA66C2–E12 was higher than other nanocomposites with same inorganic content of 2 wt %. This improvement in the storage modulus, in spite of small clay loading, was caused by the strong interaction between the organoclay and the PA66, and better dispersity of organoclay in PA66 matrix. Thermal data concludes that the organoclay acted as a heterogeneous nucleating agent and induced the for-

mation of γ-crystalline spherulites. Clay particles in nanocomposites, at low concentration, served as nucleating agents that increase the rate of crystallization of the PA66 matrix. As a result, crystallization temperature of PA66 nanocomposites was increased relative to that of neat PA66. Static mechanical analysis reveals that young's modulus and tensile strength were enhanced by introducing organoclay. In case of PA66 nanocomposites prepared using CL30B–E12, the enhancement effect was the highest. For all types of nanocomposites, elongation at break decreased rapidly with 2 wt % inorganic content loading, but changed little for the clay loading higher than 2 wt %. It was attributed to the stiffness and large aspect ratio of silicate layers. Consequently, among three types of nanocomposites, PA66CX–E12 showed the highest improvement in various properties discussed above, while PA66CX–E23 showed inferior properties than PA66CX–E00 without epoxy resin. In conclusion, an optimum amount of epoxy resin is required to form a strong interaction with the amide group of PA66.

One of the authors (V. Sriram) thanks the Ministry of Education (BK 21) fellowship.

References

1. Liu, L.; Qi, Z.; Zhu, X. J Appl Polym Sci 1999, 71, 1133.
2. Wang, Z.; Pinnavaia, T. J. Chem Mater 1998, 10, 3769.
3. Hu, Y.; Wang, S.; Ling, Z.; Zhuang, Y.; Chen, Z.; Fan, W. Macromol Mater Eng 2003, 288, 272.
4. Schmidt, D.; Shah, D.; Giannelis, E. P. Curr Opin Solid State Mater Sci 2002, 6, 205.
5. Yano, K.; Usuki, A.; Okada, A.; Kurauchi, T.; Kamigaito, O. J Polym Sci Part A: Polym Chem 1993, 31, 2493.
6. Messersmith, P. B.; Giannelis, E. P. J Polym Sci Part A: Polym Chem 1995, 33, 1047.
7. Chen, W.; Xu, Q.; Yuan, R. Z. Mater Sci Eng B 2000, 77, 15.
8. Chen, W.; Xu, Q.; Yuan, R. Z. Compos Sci Technol 2001, 61, 935.
9. Yoon, P. J.; Fornes, T. D.; Paul, D. R. Polymer 2002, 43, 6727.
10. Kawasumi, M. J Polym Sci Part A: Polym Chem 2004, 42, 819.
11. Usuki, A.; Koiwai, A.; Kojima, Y.; Kawasumi, M.; Okada, A.; Kurauchi, T.; Kamigaito, O. J Appl Polym Sci 1995, 55, 119.
12. Kojima, Y.; Usuki, A.; Kawasumi, M.; Okada, A.; Kurauchi, T.; Kamigaito, O. J Polym Sci Part A: Polym Chem 1993, 31, 983.
13. Kojima, Y.; Usuki, A.; Kawasumi, M.; Okada, A.; Kurauchi, T.; Kamigaito, O. J Appl Polym Sci 1993, 49, 1259.
14. Kojima, Y.; Fukumori, K.; Usuki, A.; Okada, A.; Kurauchi, T. J Mater Sci Lett 1993, 12, 889.
15. Usuki, A.; Kojima, Y.; Kawasumi, M.; Okada, A.; Fukushima, Y.; Kurauchi, T.; Kamigaito, O. J Mater Res 1993, 8, 1179.
16. Okada, A.; Usuki, A. Mater Sci Eng C 1995, 3, 109.
17. Cho, J. W.; Paul, D. R. Polymer 2001, 42, 1083.
18. Fornes, T. D.; Yoon, P. J.; Keskkula, H.; Paul, D. R. Polymer 2001, 42, 9929.
19. Goettler, L. U.S. Pat. WO 99/41299 (1999).
20. Goettler, L.; Joardar, S.; Middleton, J. US Pat. WO 00/09571 (2000).
21. Lu, Y.; Zhang, G.; Feng, M.; Zhang, Y.; Yang, M.; Shen, D. J Polym Sci Part B: Polym Phys 2003, 41, 2313.
22. Liu, X.; Wu, Q.; Berglund, L. Polymer 2002, 43, 4967.
23. Liu, X.; Wu, Q.; Zhang, Q.; Mo, Z. J Polym Sci Part B: Polym Phys 2003, 41, 63.
24. Wu, T.; Wu, J. J Macromol Sci Phys 2002, 41, 17.
25. Zhang, Q.; Yu, Z.; Yang, M.; Ma, J.; Mai, Y. J Polym Sci Part B: Polym Phys 2003, 41, 2861.
26. Qin, H.; Su, Q.; Zhang, S.; Zhao, B.; Yang, M. Polymer 2003, 44, 7533.
27. Yu, Z.; Yang, M.; Zhang, Q.; Zhao, C.; Mai, Y. J Polym Sci Part B: Polym Phys 2003, 41, 1234.
28. Liu, X.; Wu, Q. Macromol Mater Eng 2002, 287, 180.
29. Nair, S.; Goettler, L. A.; Lysek, B. A. Polym Eng Sci 2002, 42, 1872.
30. Han, B.; Ji, G.; Wu, S.; Shen, J. Eur Polym J 2003, 39, 1641.
31. Tanaka, G.; Goettler, L. A. Polymer 2002, 43, 541.
32. Sasgupta, S.; Hammond, W. B.; Goddard, W. A. J Am Chem Soc 1996, 118, 12291.
33. Lu, S.; In, Y. P.; Ling, C.; Tianxi, L.; Kaiyang, Z. Polymer 2004, 45, 3341.
34. Inoue, M. J Polym Sci Part A: Polym Chem 1963, 1, 2697.
35. Campoy, I.; Gomez, M. A.; Macro, C. Polymer 1998, 39, 6279.
36. Wu, T. M.; Chen, E. C.; Liao, C. S. Polymer Eng Sci 2002, 42, 1141.
37. Liu, X.; Wu, Q. Polymer 2002, 43, 1933.
38. Noh, M. H.; Jang, L. W.; Lee, D. C. J Appl Polym Sci 1994, 74, 179.
39. Zanetti, M.; Camino, G.; Thomann, R.; Mülhaupt, R. Polymer 2001, 42, 4501.
40. VanderHart, D. L.; Asano, A.; Gilman, J. W. Chem Mater 2001, 13, 3796.
41. Ray, S. S.; Okamoto, M. Prog Polym Sci 2003, 28, 1539.